ACS APPLIED MATERIALS & INTERFACES

Research Article

Cite This: ACS Appl. Mater. Interfaces 2017, 9, 43886−43892

www.acsami.org

Role of Polymer Segregation on the Mechanical Behavior of All-Polymer Solar Cell Active Layers

Nrup Balar,[†] Yuan Xiong,[‡] Long Ye,[‡] Sunsun Li,[§] Daniel Nevola,[‡] Daniel B. Dougherty,[‡] Jianhui Hou,[§] Harald Ade,[‡] and Brendan T. O'Connor*[,†]

[†]Department of Mechanical and Aerospace Engineering and [‡]Department of Physics, Organic and Carbon Electronics Laboratory (ORaCEL), North Carolina State University, Raleigh, North Carolina 27695, United States

[§]State Key Laboratory of Polymer Physics and Chemistry, Beijing National Laboratory for Molecular Sciences, Institute of Chemistry, Chinese Academy of Sciences, Beijing 100190, P. R. China

Supporting Information

ABSTRACT: An all-polymer bulk heterojunction (BHJ) active layer that removes the use of commonly used small molecule electron acceptors is a promising approach to improve the thermomechanical behavior of organic solar cells. However, there has been limited research on their mechanical properties. Here, we report on the mechanical behavior of high-performance blade-coated all-polymer BHJ films cast using eco-friendly solvents. The mechanical properties considered include the elastic modulus, crack onset strain, and cohesive fracture energy. We show that the mechanical behavior of the blend is largely unaffected by significant changes in the segregation characteristics of the polymers, which was varied systematically through solvent formulation. In comparison to a polymer:fullerene BHJ counterpart, the all-polymer films were found to have lower stiffness and increased ductility. Yet, the fracture energy of the all-polymer films is not significantly improved compared to that of the polymer:fullerene films. This study highlights that improved mechanical behavior of all-polymer systems cannot be assumed, and that details of the molecular structure, molecular weight, and film morphology play an important role in both the optoelectronic and mechanical properties. Furthermore, we show that simple composite modeling provides a predictive tool for the mechanical properties of the polymer blend films, providing a framework to guide future optimization of the mechanical behavior.

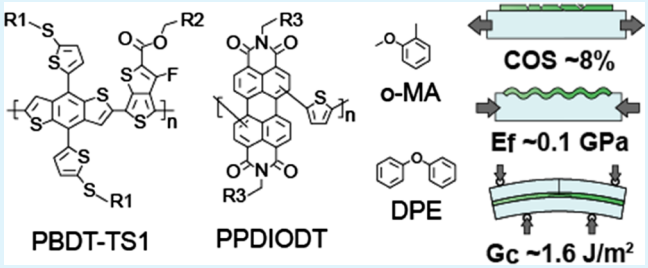

KEYWORDS: *all-polymer solar cell, polymer blend film, fracture energy, crack onset strain, multilength scale morphology*

INTRODUCTION

Organic semiconductors are compliant materials that are processed as thin films at moderate temperatures often onto plastic substrates enabling highly flexible devices.[1,2] In organic solar cells (OSCs), flexibility can be exploited for a broad range of applications from conformal energy harvesters for wearable electronics to remote power sources that can be easily stowed. However, thermomechanical failure has been found to be a common degradation path in flexible OSCs.[3,4] In response, establishing the role of the constituent materials and film morphology on mechanical stability and approaches to improve stability has been gaining interest.[5−7] To date, the majority of OSC demonstrations employ an electron donor polymer with electron acceptor fullerene to form a bulk heterojunction (BHJ) film. However, the addition of fullerene acts as an antiplasticizer and significantly degrades the mechanical stability of the film.[6,8,9] In addition, fullerenes have limited absorption and inability to tune energy levels that hinder advancements in solar cell efficiency.[10,11] Alternatively, nonfullerene small molecule acceptors have been developed that have led to recent solar cell performance gains, but they can also embrittle the film.[12,13] A promising alternative approach to improve both the solar cell performance and the mechanical behavior is through employing polymer semiconductors for both the electron donor and acceptor.[14]

All polymer solar cells (all-PSCs) have recently seen significantly improved power conversion efficiencies,[15,16] attributed to tuned electronic properties and processing methods to attain efficient BHJ morphologies.[17,18] All-PSCs have also been reported with improved ductility and toughness compared to their polymer:fullerene counterpart.[14] This was generally associated with improved molecular mobility of polymers compared to small molecules and the ability to form molecular entanglements. Although all-PSCs are promising material systems for mechanically robust flexible OSCs, there have been limited studies on the mechanical behavior of these systems. The polymers employed and the film morphology in particular may have a significant impact on the mechanical

Received: September 9, 2017
Accepted: November 30, 2017
Published: November 30, 2017

DOI: 10.1021/acsami.7b13719
ACS Appl. Mater. Interfaces 2017, 9, 43886−43892

behavior of the film. This has been shown to be the case in polymer:fullerene OSCs[8,19] and, more generally, in binary blends of polymers.[20−22] Here, we consider the mechanical behavior of a high-performance all-PSC material system and the role of film morphology on its mechanical behavior. We also compare the mechanical properties of the all-polymer active layer with an analogous polymer:fullerene active layer. The mechanical properties measured include the elastic modulus (E_f), crack onset strain (COS), and cohesive fracture energy (G_c). E_f and COS provide metrics of film stiffness and ductility, whereas G_c informs the ability of the film to resist crack propagation under an applied load (e.g., flexure).[6] To the authors' knowledge, this is the first study of cohesive fracture energy for all-PSC films.

As OSCs approach commercial relevance, it is important that studies move toward processing strategies that translate to mass production. This includes fabrication of OSCs that employ roll-to-roll printing methods or scalable prototyping techniques such as blade coating.[23,24] In addition, transitioning away from the commonly used halogenated solvents to ones that are more eco-friendly will further improve commercialization prospects.[25,26] Thus, we focus on an all-PSC system processed using blade coating, with the polymers dissolved in eco-friendly solvents, as illustrated in Figure 1a.

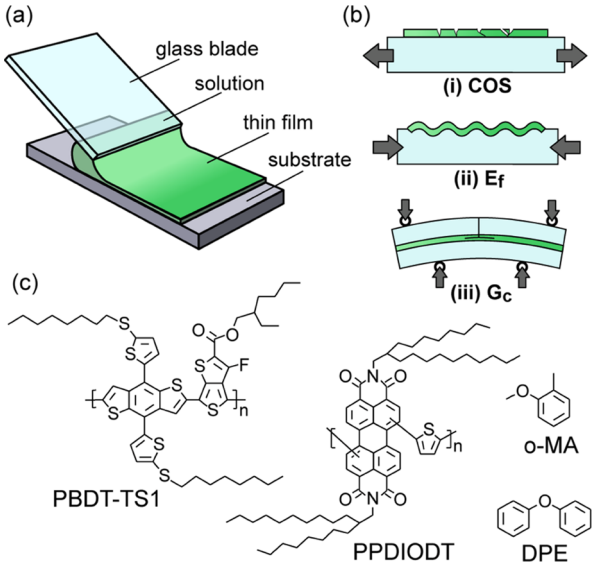

Figure 1. (a) Schematic of the blade-coating process. (b) Schematic of the film on elastomer tests under applied tension to determine COS (i) and under compression to determine elastic modulus (ii). Illustration of four-point bending (FPB) is also shown to determine the cohesive fracture energy (iii). (c) Molecular structure of the polymers PBDT-TS1 and PPDIODT and the solvent *o*-MA and the solvent additive DPE.

Here, we varied the amount of the solvent additive, diphenyl ether (DPE), to systematically manipulate the morphology of blade-coated PBDT-TS1:PPDIODT BHJ films processed in *o*-methylanisole (*o*-MA). The morphology of the films was previously characterized using atomic force microscopy (AFM), grazing incidence wide-angle X-ray scattering (GIWAXS), resonant soft X-ray scattering (R-SoXS),[27] and variable angle spectroscopic ellipsometry (VASE) measurements.[28] The GIWAXS results indicated that the polymers in the blend film are weakly crystalline, with little out-of-plane stacking preference independent of the amount of the DPE additive employed. However, a hierarchical morphology with domains at two distinct length scales was observed, as probed by R-SoXS, where a variation in domain spacing was observed with the amount of DPE. There were small domains that had a characteristic spacing of ∼14 nm for all amounts of DPE and large domains with spacing that varied from ∼140 to ∼280 nm as the amount of DPE increased from 0 to 5%, with results summarized in Table 1.[28] The increase in the large domain size

Table 1. Summary of Morphological Data Obtained from R-SoXS Profiles[a]

solvent	DPE (vol %)	large domain spacing [nm]	small domain spacing [nm]	large domain volume fraction (φ_l)
MA + 0% DPE	0	139.9	13.3	0.02
MA + 0.5% DPE	0.5	188.7	13.7	0.04
MA + 2% DPE	2.0	264.0	14.1	0.11
MA + 5% DPE	5.0	275.6	14.2	0.22

[a]Data adapted from ref 25.

was found to coincide with an increase in volume fraction of the large domains relative to the small domains, from approximately 2 to 22%, as given in Table 1. No change in purity of the large and small domains was observed with a change in domain spacing. The increase in the size of the large domains had a detrimental effect on the performance of the solar cells as summarized in Figure S1b.

In this study, we find that polymer blend films have greater compliance (lower elastic modulus) and ductility (larger COS) compared to polymer:fullerene films with an identical donor, while the cohesive fracture energy of the two systems are similar and relatively poor. We also find that the phase segregation behavior of the polymer blends does not have a large impact on the mechanical behavior. Finally, we discuss the origins of this behavior and approaches to improve the mechanical behavior.

EXPERIMENTAL METHODS

Film Preparation. The all-PSC consists of the electron donor poly{[4,8-bis[5-(octylthio)-thiophene-2-yl]benzo[1,2-*b*:4,5-*b*′]-dithiophene-2,6-diyl]-*alt*-[2-ethylhexyl-3-fluorothieno[3,4-*b*]-thiophene-2-carboxylate]} (PBDT-TS1) and the acceptor poly{[*N*,*N*′-bis(2-octyldodecyl)-3,4,9,10-perylene diimide-1,7-diyl]-*alt*-(thiophene-2,5-diyl)} (PPDIODT). Both the PBDT-TS1 (M_n = 29 kDa; PDI = 2.2)[29] and PPDIODT (M_n = 13.6 kDa; PDI = 1.38)[30] were synthesized using previously described methods. The films are processed using the eco-friendly solvent *o*-MA and the solvent additive DPE. The molecular structure of the polymers and solvents is given in Figure 1c. We have previously shown that this material system and the processing approach can achieve high efficiencies for blade-coated all-PSCs of approximately 5.6%.[26] We have also shown that the use of the additive DPE can precisely manipulate features of the complex BHJ morphology, which is discussed further below.[28] Polymer:fullerene BHJ films are also prepared by blending PBDT-TS1 with [6,6]-phenyl-C_{71}-butyric acid methyl ester ($PC_{71}BM$) in different ratios.[30] $PC_{71}BM$ (purity > 99%) was purchased from Nano-C. The solvent *o*-MA and the solvent additive DPE were purchased from Sigma-Aldrich.

Sample preparation was started by spin-casting poly(3,4-ethylenedioxythiophene):polystyrene sulfonate (PEDOT:PSS) (AI 4083, Heraeus) at 5000 rpm for 60 s on a substrate (glass or silicon) that is then annealed at 120 °C for 20 min in air, which resulted in a 35 nm thick film. The PBDT-TS1:PPDIODT films were then blade-coated in

DOI: 10.1021/acsami.7b13719
ACS Appl. Mater. Interfaces 2017, 9, 43886−43892

a ratio of 1:1 by a weight solution in *o*-MA at a total concentration of 14 mg/mL. The solution was prepared in the primary solvent *o*-MA with different amounts of DPE (0, 0.5, 2, and 5% by volume). The films were blade-coated using a blade gap of 100 μm, a substrate temperature of 80 °C, and a blade speed of 75 mm/s.[26] This resulted in a film thickness of 110 nm. The polymer:fullerene BHJ films consisted of PBDT-TS1:$PC_{71}BM$ cast in ratios of 1:1 and 1:1.5 by a weight solution at a concentration of 8 mg/mL in the solvent *o*-MA. These films were blade-coated by maintaining a blade gap of 200 μm, a substrate temperature of 70 °C, and a blade speed of 120 mm/s to achieve 90 nm film thickness. The thickness was measured using VASE (J.A. Woollam M2000).

Mechanical Characterization. COS and elastic modulus were measured by manipulating the film while on a host elastomer substrate polydimethylsiloxane (PDMS). The PDMS was cured with a base to cross linker ratio of 15:1. PDMS was laminated to the samples that consisted of the BHJ film, a PEDOT:PSS film, and the Si substrate. The stack was then immersed in water, resulting in dissolution of PEDOT:PSS and detachment of the Si substrate. COS was determined by uniaxially stretching the PDMS substrate until cracks in the film were observed through an optical microscope, illustrated in Figure 1b. The elastic modulus was calculated using a buckling-based measurement technique described in detail elsewhere.[31] In this approach, the film-elastomer stack is placed in compression resulting in film buckling, as illustrated in Figure 1b. The plane strain elastic modulus of the film ($\overline{E_f}$) is then calculated from

$$\overline{E_f} = 3\overline{E_s}\left(\frac{\lambda_B}{2\pi t}\right)^3 \quad (1)$$

where λ_B is the buckling wavelength, $\overline{E_s}$ is the plane strain elastic modulus, and t is the thickness of the substrate. The plane strain elastic modulus is given by $\overline{E} = E/(1-\nu^2)$, where E is the elastic modulus and ν is the Poisson's ratio. The Poisson's ratio of all BHJ films was taken as 0.35 and that of PDMS was taken as 0.5. The elastic modulus of a PDMS substrate was measured using a standard tensile test approach.

The cohesive fracture energy of the films was measured using a FPB test method, as illustrated in Figure 1b. The specimen consisted of a stack of films that included PEDOT:PSS followed by the BHJ film, processed as described above. Ca (20 nm) and Al (100 nm) were then thermally evaporated on the samples. The stack is then sandwiched with a glass slide, which is of the same dimensions as the substrate, and adhered through the addition of a brittle epoxy layer (EPO-TEK 353-ND). The layer of epoxy was thermally cured at 80 °C for 1 h. The metal layers help eliminate epoxy diffusion into the film of interest and act as a neighboring elastic layer.[19,32] The glass sandwich structure was then diced into FPB specimens and tested using methods previously described in detail.[33] The load−displacement curve from the FPB tests was used to calculate the critical fracture energy from the relation[19,32]

$$G_c = \frac{21P_c^2L^2}{16b^2h^3\overline{E}} \quad (2)$$

where P_c is the critical load, L is the distance between the inner pin and the outer pins, b is the width, and h is the half thickness of the test specimens. The elastic modulus of the glass was taken as 70 GPa and Poisson's ratio as 0.24. Cohesive failure was confirmed by visual inspection and through AFM analysis. All mechanical tests were conducted in air at room temperature.

EXPERIMENTAL RESULTS

Film Stiffness and Ductility. The COS and elastic modulus of the polymer blend films as a function of the amount of DPE are given in Figure 2. It was found that the COS and E_f of the polymer blend films are largely independent of the amount of DPE in the solution. For all of the polymer blend films, the COS was found to be approximately 8%, and the E_f was approximately 0.1 GPa. For comparison, COS and E_f were also measured for neat PBDT-TS1 and PPDIODT films. The COS of PBDT-TS1 films was found to be 23%, whereas for

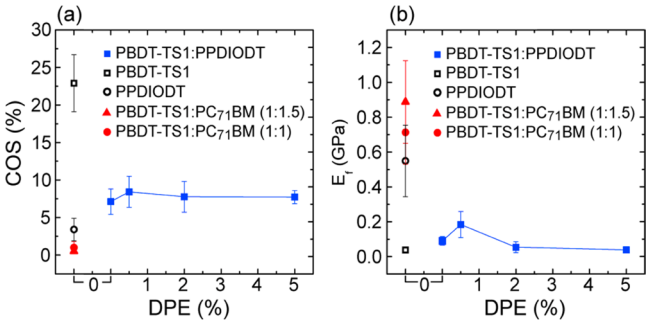

Figure 2. (a) COS and (b) elastic modulus (E_f) of neat polymer films, polymer:fullerene films, and all-polymer films cast from solution with varying amounts of DPE. Average COS and E_f for each data point are calculated from a minimum of four samples. Uncertainties were determined as 1 SD of the mean.

PPDIODT films, COS was 3.4%. The COS of the blend films is found to be between the neat films, with a value closer to the neat PPDIODT film (Figure 2). The E_f of the blend film is also found to be between the elastic modulus of the neat polymer films and close to the lower modulus PBDT-TS1. These results are consistent with a composite model discussed in further detail below. In comparison, polymer:fullerene (PBDT-TS1:$PC_{71}BM$) blends were found to be stiffer and more brittle as shown in Figure 2, which is consistent with other reports of polymer:fullerene films.[8,9,14] This is attributed to the stiff and brittle nature of fullerenes, where COS and E_f of neat fullerene thin films have previously been reported to be <1% and approximately 3.1 GPa, respectively.[8] The change in the mechanical behavior of the polymer blend film when adding fullerene is generally associated with an increase in the glass transition temperature (T_g).[8]

Optimum solar cell performance of PBDT-TS1:$PC_{71}BM$ has been shown to be at the blend ratio of 1:1.5.[30] However, increasing the fraction of $PC_{71}BM$ is expected to be detrimental to the mechanical behavior, and thus, polymer:fullerene ratios of 1:1 and 1:1.5 were both considered. Indeed, we found that the increase in $PC_{71}BM$ resulted in increased stiffness and lower ductility of the polymer:fullerene films. The 1:1 and 1:1.5 polymer:fullerene blends exhibited a COS of 1.0 and 0.5% and an E_f of 0.7 and 0.9 GPa, respectively. Both polymer:-fullerene films had unstable cracks that propagated across the film once formed, and there were no distinguishable differences in crack features.

Fracture Energy. The cohesive fracture energies of the all-polymer films were also found to be fairly invariant with the amount of DPE employed, with all films having a fracture energy between 1.6 and 2.0 J/m^2 as given in Figure 3. This fracture energy is relatively poor, where in comparison tough cross-linked polymer films can have fracture

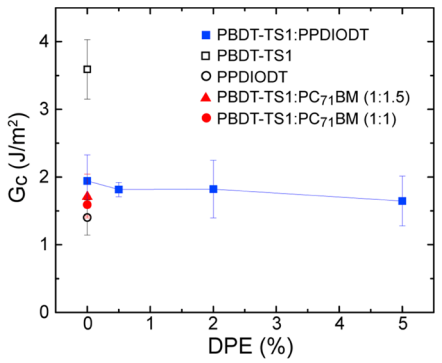

Figure 3. Cohesive fracture energy (G_c) of neat polymer films, polymer:fullerene films, and all-polymer films cast from solution with varying amounts of DPE. The fracture energy is calculated from a minimum of four samples. Uncertainties were determined as 1 SD of the mean.

DOI: 10.1021/acsami.7b13719
ACS Appl. Mater. Interfaces 2017, 9, 43886−43892

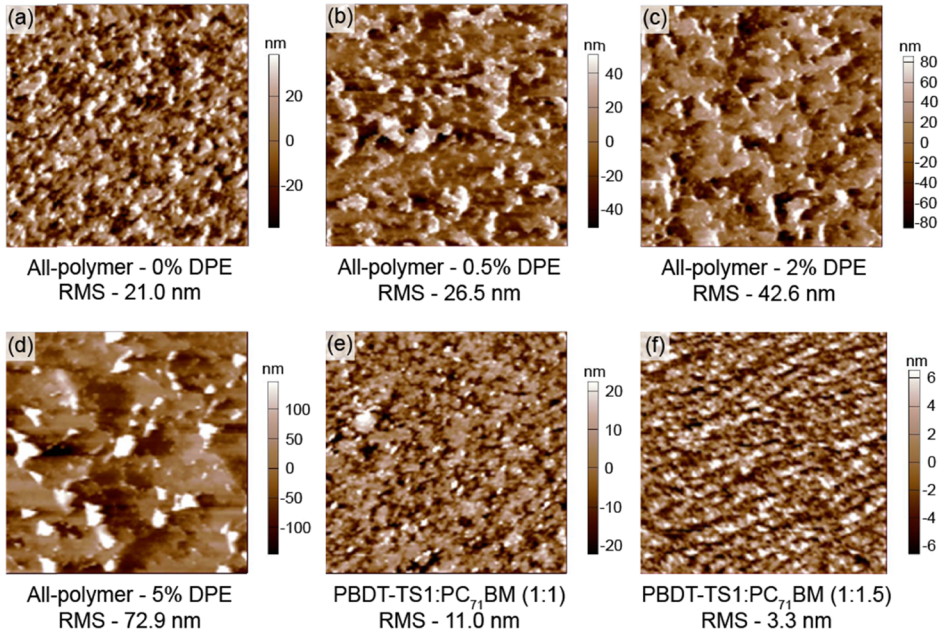

Figure 4. AFM scans of fractured surfaces of all-polymer films cast (a) without a solvent additive and (b) 0.5%, (c) 2%, and (d) 5% DPE. AFM scans of fractured surfaces corresponding to blend films of PBDT-TS1:$PC_{71}BM$ with blend ratios of (e) 1:1 and (f) 1:1.5 by mass. rms roughness of each surface is indicated under the image of each scan. The size of each scan is 10 μm × 10 μm. All scans were performed in the region where crack propagated near mid-film thickness.

energies significantly greater than ~10 J/m^2 at similar film thicknesses.[19] Although the application and the device architecture will dictate mechanical stability, the low fracture energy suggests that these films will be prone to mechanical failure in flexible solar cell applications. The fracture energy of the blend films was closer to that measured for neat PPDIODT films, which is similar to COS (Figure 3). Visually, striation marks were observed at the fractured surfaces, which are often associated with a stick-slip phenomenon during crack propagation, which is consistent with the saw-tooth load versus displacement profile observed in the FPB tests.[34,35] The striation marks were from the crack jumping from the middle of the film to much closer to the Ca interface during propagation. To gain a clearer view of the fracture surface, they were probed by AFM. The scans showed a rougher surface when the crack propagated near the center of the film as compared to when crack propagation was close to the Ca interface. The mid-plane crack propagation was found to be ~60 nm from the PEDOT:PSS interface for all amounts of DPE (as shown in Figure S3). In the mid-plane fracture region, it was found that the roughness of the fracture interface increases with the increase in the amount of DPE in the solution, as shown in Figure 4. Generally, an increase in the roughness of a fractured surface is associated with an increase in fracture energy.[32,36] In these cases, the increased roughness is associated with an increase in the plastic zone or crazing near the crack tip. However, given the similar G_c and COS between films studied here, it is suspected that there is not a large change in plasticity among the films. Thus, the change in surface roughness observed between films is attributed to the differences in film morphology. The crack will propagate along the weakest path (e.g., chain pullout along segregated domains), and this path likely changes with the change in segregation characteristics in the films. This is consistent with molecular dynamic simmulations by Tummala et al. who showed that mixing of the components in a blend film affects the fracture energy and the region through which the crack propagates.[37] The trend in surface roughness is consistent with the change in the larger domain size observed by R-SoXS, although the characteristic size scale in the AFM images is significantly larger than the domain spacing. For comparison, AFM scans of the fractured surface of neat PBDT-TS1 and PPDIODT are given in Figure S4. The PBDT-TS1 had a rougher fracture surface and greater fracture energy (G_c = 3.45 J/m^2) as compared to the PPDIODT (G_c = 1.40 J/m^2) films.

In comparison to the all-polymer films, the fracture energy of PBDT-TS1:$PC_{71}BM$ blend films with blend ratios 1:1 and 1:1.5 were observed to be 1.6 and 1.7 J/m^2, respectively. Neat fullerene films have been previously reported to have a fracture energy of approximately 0.5 J/m^2.[19] The fracture energy of the polymer:fullerene films shows only a slight decrease compared to the all-polymer blend films. The low fracture energy was found along with a relatively smooth fracture surface, as shown in Figure 4. The fracture surface of the polymer:fullerene films also had fine striation marks with the crack propagation alternating between ~45 nm from the PEDOT:PSS interface and jumping to the Ca interface for both the blend ratios. A thickness dependence of the fracture energy for the polymer:fullerene blends was also studied with results given in Figure S5. There was no significant variation in fracture energy with thickness, which is consistent with a little plastic deformation near the crack tip.[32] Similarly, the relatively low fracture energy of the all-polymer blend film suggests that there is no significant amount of plastic deformation near the crack tip that would dissipate the stress concentration. This behavior is consistent with the relatively low COS measured in these films.[33]

The fracture surfaces of the all-polymer films were further probed by X-ray photoelectron spectroscopy (XPS) to determine the molecular composition of each surface, with details provided in the Supporting Information. It was found that both sides of the fracture surface had a similar composition and was PBDT-TS1-rich. The PBDT-TS1:PPDIODT monomer ratio was found to increase from approximately 1.3:1 to 2.5:1 with increasing DPE in the solution. The fracture surface having a greater fraction of PBDT-TS1 is likely associated with vertical segregation of the polymers in the films. Previously, it was found that spin-cast PBDT-TS1:PPDIODT films showed a vertical segregation behavior with preferential segregation of PBDT-TS1 toward the Ca interface and PPDIODT toward the PEDOT:PSS interface.[29] As noted above, the fracture surface alternated between the middle of the film to much closer to the Ca interface. The X-ray spot size covered both the mid-film and near-surface fracture surfaces. The XPS results suggest that there is also vertical segregation in the blade-cast films considered here, and that we are measuring the PBDT-TS1 enrichment near the Ca interface. While enrichment of PBDT-TS1 was found, there was also a substantial amount of PPDIODT, suggesting that fracture did not propagate

DOI: 10.1021/acsami.7b13719
ACS Appl. Mater. Interfaces 2017, 9, 43886−43892

primarily through a pure polymer phase associated with material segregation.

DISCUSSION

To gain insight into the mechanical behavior of the blend, it is instructive to consider composite models that have been successfully applied to binary polymer blends.[20] A simple model to consider the mechanical limits would be to consider the blend as a composite composed of the two polymers purely in parallel or series. An advancement of this simple picture is to consider an equivalent box model (EBM) that consists of a volume fraction of the composite that acts in parallel and a volume fraction that acts in series.[20] The EBM has been shown to predict the elastic modulus and tensile strength of immiscible polymer blends well, as long as the mixing process does not significantly alter the mechanical behavior of the components (e.g., change in crystallinity). Here, we predict the elastic modulus and fracture energy of the blend films using the EBM. The model is applied with a series component, that is, approximately 70% by volume. This is determined by using model inputs that have been shown to fit experimental results of a variety of polymer blends well,[20] with additional details provided in the Supporting Information. Applying the composite model to the elastic modulus of the blend film, we find that a simple parallel composite model predicts an elastic modulus of 0.07 GPa, and the EBM estimates an elastic modulus of 0.12 GPa. Both are in the range of the measured elastic modulus of 0.04 to 0.18 GPa.

When considering cohesive fracture energy, we apply the same composite model used to estimate the elastic modulus. Importantly, polymer blends can have elongations at break (and by extension, COS and G_c) that range from below the lower limit of the neat polymer films to values approaching that of the high ductility polymer constituent.[20,21,38] This is associated with the ability to transfer stress between segregated domains that is driven by interfacial adhesion. The EBM is able to capture the role of interfacial adhesion with the upper and lower limits of perfect adhesion and zero adhesion between components, respectively.[20] Applying the EBM to the all-polymer system, we predict a fracture energy of 2.13 J/m^2, which compares well to the measured fracture energy that ranged from 1.65 to 1.94 J/m^2. When considering interfacial adhesion, the fracture energies were bound between 0.76 and 3.1 J/m^2. These results along with the COS of the polymer blend, being closer to the lower ductility PPDIODT, suggest that there is limited stress transfer between polymer components. Applying the EBM to polymer:fullerene films, we also estimate the elastic modulus and fracture energy well, with details given in the Supporting Information. It should be noted that further research exploring different polymer ratios is necessary to validate the composite model fully. In addition, the miscibility of the components will affect intermolecular interactions and, subsequently, the mechanical properties.[37] However, the model does not include interaction terms that would assist in capturing miscibility, changes in film density, and other important morphological factors.[39] Nevertheless, the model is found to fit the experimental data well. Remarkably, this occurs for the all-polymer blend that has limited segregation of pure domains and with the majority of the film being composed of small characteristics domains spaced by roughly 14 nm.

The ability to successfully apply this composite model highlights the need to maximize the mechanical behavior of the constituent polymers. In considering the mechanical behavior of polymers, key parameters include the molecular weight, glass transition temperature, intermolecular bond strength, and crystallinity.[8,32,40−42] For the polymers considered here, the molecular weight of both polymers is relatively low, likely limiting intermolecular entanglements that would improve the toughness of the film. PPDIODT has a particularly low molecular weight that is likely to be a significant contributing factor to the low COS and fracture energy of the neat PPDIODT films. The lack of entanglements would limit stress transfer near the crack tip and result in low fracture energy. This is consistent with the poor stress transfer predicted by the composite modeling.

For comparison, Kim et al. recently reported the stress−strain behavior of all-PSC BHJ films that consisted of similarly structured polymers PBDTTTPD and P(NDI2HD-T).[14] In their report, the tensile tests were performed on quasifree standing films by floating them on water during testing.[14] They reported an elastic modulus of 0.43 GPa and an elongation at break of 7%. They also observed that the polymer:fullerene counterpart was stiffer (0.8−1.76 GPa) with an elongation at break of 0.1−0.3%. Their reported elastic moduli compare well to our film-buckling measurements, where we find an elastic modulus of 0.04−0.18 GPa for the polymer blend and 0.8−0.9 GPa for the polymer:fullerene film. The elongation at break of their polymer blend also compared well with our COS measurements. However, the COS is not equivalent to the elongation at break, as the elastomer substrate can influence the point of fracture.[43] In a recent study comparing the film on elastomer COS to the film on water elongation at break, the COS was consistently greater than the elongation at break.[43] This suggests that the all-polymer film reported by Kim et al. had greater ductility than the films reported here. Comparing the two polymer blends, in the report by Kim et al., the acceptor polymer [P(NDI2HD-T)] had a much higher molecular weight (M_n = 48 kDa) compared to PPDIODT (13.6 kDa). While further research is required to distinguish other contributing factors such as the molecular structure and film morphology, the molecular weight appears to be an important contributing factor. This is supported by other studies of polymer:fullerene blend films, where the polymer molecular weight was shown to impact the fracture energy significantly because of a significant increase in entanglements of polymer chains.[32,37]

CONCLUSIONS

The mechanical properties of high-performance all-PSC BHJ films were characterized by measuring COS, elastic modulus, and cohesive fracture energy. These films were cast using the scalable method of blade-coating using eco-friendly solvents. The morphology of the films was finely tuned through the use of a benign solvent additive. The mechanical properties were then compared to films composed of the individual polymer components as well as comparable polymer:fullerene BHJ films. The results showed that the all-PSC has greater compliance and ductility than its polymer:fullerene counterpart. However, the fracture energy of the all-PSC films was found to be relatively poor and not substantially better than the polymer:fullerene films. Importantly, FPB tests lead to a mixed load failure mode that compliments the loading conditions that would likely be encountered for a heterogeneous device stack under flexure.[19] The low fracture energy suggests that the all-PSCs reported here may be prone to fracture during device operation.

DOI: 10.1021/acsami.7b13719
ACS Appl. Mater. Interfaces 2017, 9, 43886−43892

It was shown that a simple composite model predicts the mechanical behavior of the polymer blend film well. The composite model highlights the importance of optimizing the mechanical performance of the individual polymers to be applied in the all-PSCs. In the polymers considered here, the stiff polymer backbone and low molecular weight are believed to limit chain entanglements, leading to the low COS and fracture energy. It is expected that selecting polymers taking into account both mechanical and optoelectronic properties will lead to significant advances in achieving high-performance physically robust flexible OSCs.

■ ASSOCIATED CONTENT

Supporting Information

The Supporting Information is available free of charge on the ACS Publications website at DOI: 10.1021/acsami.7b13719.

XPS analysis, thickness measurement by AFM, AFM scans of neat polymer films, G_c of PBDT-TS1:$PC_{71}BM$ blend films versus film thickness, E_f of all-polymer blend films, and description of the composite model of the mechanical behavior (PDF)

■ AUTHOR INFORMATION

Corresponding Author

*E-mail: btoconno@ncsu.edu.

ORCID

Sunsun Li: 0000-0003-3581-8358

Daniel B. Dougherty: 0000-0002-5016-0913

Jianhui Hou: 0000-0002-2105-6922

Brendan T. O'Connor: 0000-0002-8999-5184

Notes

The authors declare no competing financial interest.

■ ACKNOWLEDGMENTS

The authors gratefully acknowledge support for this research through NSF CAREER award 1554322 and NSF INFEWS/T3 grant 1639429. The DTS and VASE measurements were made possible through support from the UNC-General Administration Research Opportunity Initiative. Research at the Hou lab was carried out with the financial support from NSFC (21325419, 91333204). Acquisition of R-SoXS data at beamline 11.0.1.2 at the Advanced Light Source (ALS) in Berkeley National Lab was supported by the U.S. Department of Energy (DE-AC02-05CH11231). Beamline supports at ALS by beamline scientists (C. Wang, C. Zhu, A. L. D. Kilcoyne, Y. Yu, and E. Schaible) are acknowledged. The authors would like to thank Dr. J. Muth for support with dicing the four-point bending specimens.

■ REFERENCES

(1) Kaltenbrunner, M.; White, M. S.; Głowacki, E. D.; Sekitani, T.; Someya, T.; Sariciftci, N. S.; Bauer, S. Ultrathin and Lightweight Organic Solar Cells with High Flexibility. *Nat. Commun.* **2012**, *3*, 770.

(2) Forrest, S. R. The Path to Ubiquitous and Low-Cost Organic Electronic Appliances on Plastic. *Nature* **2004**, *428*, 911−918.

(3) Krebs, F. C.; Nielsen, T. D.; Fyenbo, J.; Wadstrøm, M.; Pedersen, M. S. Manufacture, Integration and Demonstration of Polymer Solar Cells in a Lamp for the "Lighting Africa" Initiative. *Energy Environ. Sci.* **2010**, *3*, 512−525.

(4) Jørgensen, M.; Norrman, K.; Gevorgyan, S. A.; Tromholt, T.; Andreasen, B.; Krebs, F. C. Stability of Polymer Solar Cells. *Adv. Mater.* **2012**, *24*, 580−612.

(5) O'Connor, B. T.; Awartani, O. M.; Balar, N. Morphological Considerations of Organic Electronic Films for Flexible and Stretchable Devices. *MRS Bull.* **2017**, *42*, 108−114.

(6) Kim, J.-H.; Lee, I.; Kim, T.-S.; Rolston, N.; Watson, B. L.; Dauskardt, R. H. Understanding Mechanical Behavior and Reliability of Organic Electronic Materials. *MRS Bull.* **2017**, *42*, 115−123.

(7) Bao, Z.; Chen, X. Flexible and Stretchable Devices. *Adv. Mater.* **2016**, *28*, 4177−4179.

(8) Awartani, O.; Lemanski, B. I.; Ro, H. W.; Richter, L. J.; DeLongchamp, D. M.; O'Connor, B. T. Correlating Stiffness, Ductility, and Morphology of polymer:Fullerene Films for Solar Cell Applications. *Adv. Energy Mater.* **2013**, *3*, 399−406.

(9) Savagatrup, S.; Makaram, A. S.; Burke, D. J.; Lipomi, D. J. Mechanical Properties of Conjugated Polymers and Polymer-Fullerene Composites as a Function of Molecular Structure. *Adv. Funct. Mater.* **2014**, *24*, 1169−1181.

(10) Douglas, J. D.; Chen, M. S.; Niskala, J. R.; Lee, O. P.; Yiu, A. T.; Young, E. P.; Fréchet, J. M. J. Solution-Processed, Molecular Photovoltaics That Exploit Hole Transfer from Non-Fullerene, n-Type Materials. *Adv. Mater.* **2014**, *26*, 4313−4319.

(11) Fang, Y.; Pandey, A. K.; Nardes, A. M.; Kopidakis, N.; Burn, P. L.; Meredith, P. A Narrow Optical Gap Small Molecule Acceptor for Organic Solar Cells. *Adv. Energy Mater.* **2013**, *3*, 54−59.

(12) Rodriquez, D.; Savagatrup, S.; Valle, E.; Proctor, C. M.; McDowell, C.; Bazan, G. C.; Nguyen, T.-Q.; Lipomi, D. J. Mechanical Properties of Solution-Processed Small-Molecule Semiconductor Films. *ACS Appl. Mater. Interfaces* **2016**, *8*, 11649−11657.

(13) Kim, J.-H.; Noh, J.; Choi, H.; Lee, J.-Y.; Kim, T.-S. Mechanical Properties of Polymer−Fullerene Bulk Heterojunction Films: Role of Nanomorphology of Composite Films. *Chem. Mater.* **2017**, *29*, 3954−3961.

(14) Kim, T.; Kim, J.-H.; Kang, T. E.; Lee, C.; Kang, H.; Shin, M.; Wang, C.; Ma, B.; Jeong, U.; Kim, T.-S.; Kim, B. J. Flexible, Highly Efficient All-Polymer Solar Cells. *Nat. Commun.* **2015**, *6*, 8547.

(15) Gao, L.; Zhang, Z.-G.; Xue, L.; Min, J.; Zhang, J.; Wei, Z.; Li, Y. All-Polymer Solar Cells Based on Absorption-Complementary Polymer Donor and Acceptor with High Power Conversion Efficiency of 8.27%. *Adv. Mater.* **2016**, *28*, 1884−1890.

(16) Hwang, Y.-J.; Courtright, B. A. E.; Ferreira, A. S.; Tolbert, S. H.; Jenekhe, S. A. 7.7% Efficient All-Polymer Solar Cells. *Adv. Mater.* **2015**, *27*, 4578−4584.

(17) Kang, H.; Lee, W.; Oh, J.; Kim, T.; Lee, C.; Kim, B. J. From Fullerene−Polymer to All-Polymer Solar Cells: The Importance of Molecular Packing, Orientation, and Morphology Control. *Acc. Chem. Res.* **2016**, *49*, 2424−2434.

(18) Chen, J.-D.; Cui, C.; Li, Y.-Q.; Zhou, L.; Ou, Q.-D.; Li, C.; Li, Y.; Tang, J.-X. Single-Junction Polymer Solar Cells Exceeding 10% Power Conversion Efficiency. *Adv. Mater.* **2015**, *27*, 1035−1041.

(19) Brand, V.; Bruner, C.; Dauskardt, R. H. Cohesion and Device Reliability in Organic Bulk Heterojunction Photovoltaic Cells. *Sol. Energy Mater. Sol. Cells* **2012**, *99*, 182−189.

(20) Kolarik, J. Simultaneous Prediction of the Modulus and Yield Strength of Binary Polymer Blends. *Polym. Eng. Sci.* **1996**, *36*, 2518−2524.

(21) Eagan, J. M.; Xu, J.; Di Girolamo, R.; Thurber, C. M.; Macosko, C. W.; LaPointe, A. M.; Bates, F. S.; Coates, G. W. Combining Polyethylene and Polypropylene: Enhanced Performance with PE/iPP Multiblock Polymers. *Science* **2017**, *355*, 814−816.

(22) Leclair, A.; Favis, B. D. The Role of Interfacial Contact in Immiscible Binary Polymer Blends and Its Influence on Mechanical Properties. *Polymer* **1996**, *37*, 4723−4728.

(23) Shin, N.; Richter, L. J.; Herzing, A. A.; Kline, R. J.; DeLongchamp, D. M. Effect of Processing Additives on the Solidification of Blade-Coated Polymer/fullerene Blend Films via in-Situ Structure Measurements. *Adv. Energy Mater.* **2013**, *3*, 938−948.

(24) Schilinsky, P.; Waldauf, C.; Brabec, C. J. Performance Analysis of Printed Bulk Heterojunction Solar Cells. *Adv. Funct. Mater.* **2006**, *16*, 1669−1672.

(25) Venkatesan, S.; Chen, Q.; Ngo, E. C.; Adhikari, N.; Nelson, K.; Dubey, A.; Sun, J.; Bommisetty, V.; Zhang, C.; Galipeau, D.; Qiao, Q. Polymer Solar Cells Processed Using Anisole as a Relatively Nontoxic Solvent. *Energy Technol.* **2014**, *2*, 269−274.
(26) Ye, L.; Xiong, Y.; Yao, H.; Gadisa, A.; Zhang, H.; Li, S.; Ghasemi, M.; Balar, N.; Hunt, A.; O'Connor, B. T.; Hou, J.; Ade, H. High Performance Organic Solar Cells Processed by Blade Coating in Air from a Benign Food Additive Solution. *Chem. Mater.* **2016**, *28*, 7451−7458.
(27) Gann, E.; Young, A. T.; Collins, B. A.; Yan, H.; Nasiatka, J.; Padmore, H. A.; Ade, H.; Hexemer, A.; Wang, C. Soft x-ray scattering facility at the Advanced Light Source with real-time data processing and analysis. *Rev. Sci. Instrum.* **2012**, *83*, 045110.
(28) Ye, L.; Xiong, Y.; Li, S.; Ghasemi, M.; Balar, N.; Turner, J.; Gadisa, A.; Hou, J.; O'Connor, B. T.; Ade, H. Precise Manipulation of Multilength Scale Morphology and Its Influence on Eco-Friendly Printed All-Polymer Solar Cells. *Adv. Funct. Mater.* **2017**, *27*, 1702016.
(29) Li, S.; Zhang, H.; Zhao, W.; Ye, L.; Yao, H.; Yang, B.; Zhang, S.; Hou, J. Green-Solvent-Processed All-Polymer Solar Cells Containing a Perylene Diimide-Based Acceptor with an Efficiency over 6.5%. *Adv. Energy Mater.* **2016**, *6*, 1501991.
(30) Ye, L.; Zhang, S.; Zhao, W.; Yao, H.; Hou, J. Highly Efficient 2D-Conjugated Benzodithiophene-Based Photovoltaic Polymer with Linear Alkylthio Side Chain. *Chem. Mater.* **2014**, *26*, 3603−3605.
(31) Stafford, C. M.; Harrison, C.; Beers, K. L.; Karim, A.; Amis, E. J.; VanLandingham, M. R.; Kim, H.-C.; Volksen, W.; Miller, R. D.; Simonyi, E. E. A Buckling-Based Metrology for Measuring the Elastic Moduli of Polymeric Thin Films. *Nat. Mater.* **2004**, *3*, 545−550.
(32) Bruner, C.; Dauskardt, R. Role of Molecular Weight on the Mechanical Device Properties of Organic Polymer Solar Cells. *Macromolecules* **2014**, *47*, 1117−1121.
(33) Balar, N.; O'Connor, B. T. Correlating Crack Onset Strain and Cohesive Fracture Energy in Polymer Semiconductor Films. *Macromolecules* **2017**, *50*, 8611−8618.
(34) Gledhill, R. A.; Kinloch, A. J.; Yamini, S.; Young, R. J. Relationship between Mechanical Properties of and Crack Progagation in Epoxy Resin Adhesives. *Polymer* **1978**, *19*, 574−582.
(35) Hakeem, M. I.; Phillips, M. G. Unstable Crack Propagation—a Fractographic Study Using PMMA in Liquid Environments. *J. Mater. Sci.* **1979**, *14*, 2901−2905.
(36) Brand, V.; Levi, K.; McGehee, M. D.; Dauskardt, R. H. Film Stresses and Electrode Buckling in Organic Solar Cells. *Sol. Energy Mater. Sol. Cells* **2012**, *103*, 80−85.
(37) Tummala, N. R.; Bruner, C.; Risko, C.; Brédas, J.-L.; Dauskardt, R. H. Molecular-Scale Understanding of Cohesion and Fracture in P3HT:Fullerene Blends. *ACS Appl. Mater. Interfaces* **2015**, *7*, 9957−9964.
(38) Scott, J. I.; Xue, X.; Wang, M.; Kline, R. J.; Hoffman, B. C.; Dougherty, D.; Zhou, C.; Bazan, G.; O'Connor, B. T. Significantly Increasing the Ductility of High Performance Polymer Semiconductors through Polymer Blending. *ACS Appl. Mater. Interfaces* **2016**, *8*, 14037−14045.
(39) Nandan, B.; Kandpal, L. D.; Mathur, G. N. Poly(ether ether ketone)/Poly(aryl ether sulfone) Blends: Relationships Between Morphology and Mechanical Properties. *J. Appl. Polym. Sci.* **2003**, *90*, 2887−2905.
(40) Roth, B.; Savagatrup, S.; de los Santos, N. V.; Hagemann, O.; Carlé, J. E.; Helgesen, M.; Livi, F.; Bundgaard, E.; Søndergaard, R. R.; Krebs, F. C.; Lipomi, D. J. Mechanical Properties of a Library of Low-Band-gap Polymers. *Chem. Mater.* **2016**, *28*, 2363−2373.
(41) Bruner, C.; Miller, N. C.; McGehee, M. D.; Dauskardt, R. H. Molecular Intercalation and Cohesion of Organic Bulk Heterojunction Photovoltaic Devices. *Adv. Funct. Mater.* **2013**, *23*, 2863−2871.
(42) O'Connor, B.; Chan, E. P.; Chan, C.; Conrad, B. R.; Richter, L. J.; Kline, R. J.; Heeney, M.; McCulloch, I.; Soles, C. L.; DeLongchamp, D. M. Correlations between Mechanical and Electrical Properties of Polythiophenes. *ACS Nano* **2010**, *4*, 7538−7544.
(43) Rodriquez, D.; Kim, J.-H.; Root, S. E.; Fei, Z.; Boufflet, P.; Heeney, M.; Kim, T.-S.; Lipomi, D. J. Comparison of Methods for Determining the Mechanical Properties of Semiconducting Polymer Films for Stretchable Electronics. *ACS Appl. Mater. Interfaces* **2017**, *9*, 8855−8862.

DOI: 10.1021/acsami.7b13719
ACS Appl. Mater. Interfaces 2017, 9, 43886−43892